Progress In Electromagnetics Research C, Vol. 13, 135–148, 2010

ON-CHIP FGCPW LOWPASS AND BANDPASS FILTERS WITH LOW INSERTION LOSS AND HIGH STOPBAND REJECTION FOR V-BAND APPLICATIONS

H.-K. Chiou and I.-S. Chen

Department of Electrical Engineering
National Central University
No. 300, Jhongda Road, Jhongli City
Taoyuan County 32001, Taiwan, R.O.C.

Abstract—This paper presents compact on-chip finite ground coplanar waveguide (FGCPW) lowpass filter (LPF) and bandpass filter (BPF) for V-band multi gigabit per second (Gbps) wireless personal area network (WPAN) applications. The equivalent lumped-element circuit of the proposed filters can be represented by an ABCD matrix which is obtained by consecutively multiplied ABCD matrixes of one T-network impedance and two shunt admittances. The full-wave EM simulators, Ansoft^{TM} HFSS and Agilent^{TM} Momentum, were used to fine tune the desired frequency response. The FGCPW LPF and BPF were implemented in WIN^{TM} semiconductor 0.15 μm pHEMT process. The obtained insertion losses are smaller than 0.5 dB and 1.5 dB with return losses of better than 12 dB and 13 dB, respectively. The 1-dB bandwidths of the LPF and BPF are 70 GHz (0–70 GHz) and 11 GHz (55–66 GHz), respectively. The stopband rejections are better than 20 dB from 95 to 120 GHz in the LPF, and from 0 to 42 GHz and 82 to 120 GHz in the BPF. The measured frequency responses show good agreements with the simulations. The chip size is very compact of $0.43 \times 0.45\,\text{mm}^2$.

1. INTRODUCTION

The 60 GHz band is of much interest in WPAN and multi-Gbps point-to-point links for short-range multimedia wireless transmission [1]. As a peak loss in atmospheric oxygen absorption (∼15 dB/Km) occurs at 60 GHz, millimeter wave technology at 60 GHz is capable of higher capacity with better signal to interference feature than

Corresponding author: H.-K. Chiou (hkchiou@ee.ncu.edu.tw).

at the other frequencies. For these millimeter wave transceiver designs, on-chip filters are the key components that can sufficiently reject the interference signals resulting in an overall improvement of the captured multimedia quality. The principal challenges for the filter designs at millimeter-wave range are: low insertion loss, high stopband and harmonics rejections, and compact size. As the passive components, such as inductor, capacitor, resonators, and transmission lines, usually have low quality (Q) factor in millimeter-wave frequencies, the obtained insertion loss of filters is higher than that in low frequencies. Thus, the sensitivity of millimeter-wave transceiver is limited by the insertion loss of the filter. Meanwhile, the filters with high stopband and harmonic rejections are highly required to reject the strong out-of-band interferences and the spurious signals caused by nonlinear devices, such as high power amplifiers, mixers, and oscillators, etc. Since the use of on-chip filter implemented in silicon technology will lead to lower cost and higher integration level than the transceivers made by discrete components, it is also important to keep the filter size small and easy integration. Many filters operating below Ka-band are designed with CPW transmission lines to lower the insertion loss [2–6], but few 60 GHz filters have been developed by using microstrip (MS) and/or CPW transmission lines for easy integration with other RF components [7–10]. In work [7], a 60 GHz microstrip BPF has been implemented in a 0.13 μm CMOS process. The filter achieved a low insertion loss and high stopband rejection, but having a low second harmonic rejection (around 10 dB). Hsu et al. designed a microstrip BPF in 0.18 μm CMOS process [8]. However, the insertion loss was up to 4.9 dB due to the lossy substrate and the extra loss in the CPW-to-MS transition. The same drawback was found in work [9], Lee et al. used a CPW-to-slotline (SL) transition in LTCC process which BPF achieved an insertion loss of 5 dB. In work [10], a 60 GHz microstrip BPF was fabricated in GaAs processes, and achieved an excellent low insertion loss of 2.3 dB with good attenuation roll-off at the passband edges. Unfortunately, the BPF was designed for wide bandwidth response (30 GHz in passband) which is not practical for real WPAN application.

The authors propose two compact 60 GHz on-chip FGCPW LPF and BPF with lower insertion loss, higher stopband and 2nd harmonic rejections, and easier integration with SoC transceiver, compared with recently published V-band filters [7–10]. An ABCD matrix corresponded to the lumped-element equivalent circuit of the filters were used to synthesize the desired lumped-elements of the filters. For this intention, the filters are implemented using FGCPW transmission lines instead of the lumped-elements, such as on-chip capacitors,

inductors, and resonators, to obtain the compact circuit area. Hence, the chip areas of the LPF and BPF are only $0.43 \times 0.45\,\text{mm}^2$.

2. CIRCUITS DESIGN

2.1. Description of the Physical Structure

Figures 1(a) and 2(a) illustrate three-dimensional structure of the FGCPW LPF and BPF which were fabricated in WIN$^{\text{TM}}$ 0.15 µm pHEMT process. Figures 1(b) and 2(b) display the cross section of the filters. The thickness of the nitride material and GaAs substrate are 0.15 µm and 500 µm, respectively.

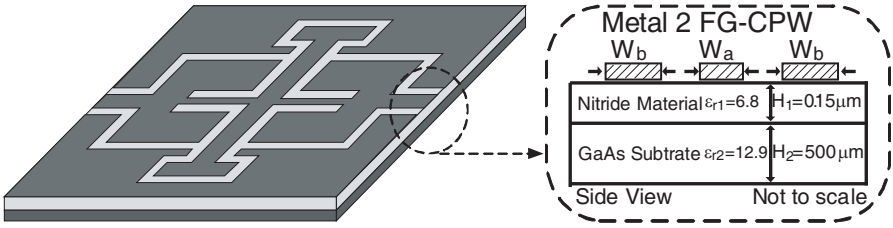

(a) (b)

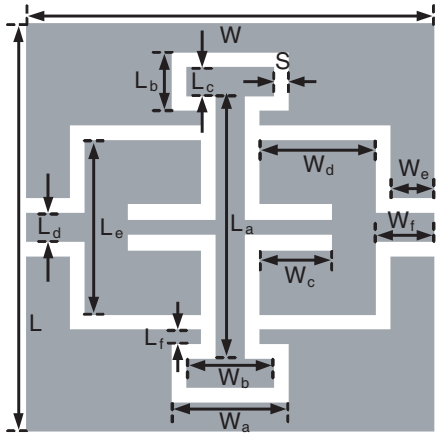

(c)

Figure 1. FGCPW LPF: (a) Three-dimensional structure, (b) cross-sectional view, and (c) top view.

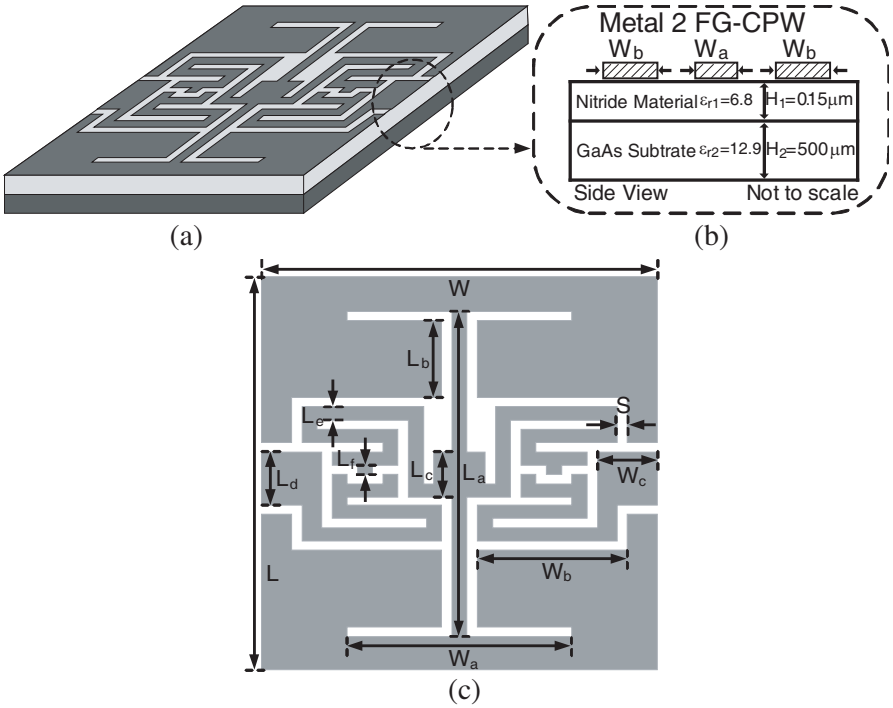

Figure 2. FGCPW BPF: (a) Three-dimensional structure, (b) cross-sectional view, and (c) top view.

Table 1. Summary of the FGCPW LPF dimensions.

Item	(μm)	Item	(μm)
L	450	W	430
L_a	285	W_a	145
L_b	70	W_b	115
L_c	40	W_c	110
L_d	55	W_d	150
L_e	170	W_e	30
L_f	25	W_f	45
S	15		

The dielectric constants of the nitride material (6.8) and GaAs substrate (12.9) are very critical in the full-wave simulations of the on-chip filter designs. An effective dielectric constant is set by taking the nitride and GaAs layers as a homogeneous substrate. This approach

Table 2. Summary of the FGCPW BPF dimensions.

Item	(μm)	Item	(μm)
L	450	L_f	15
L_a	400	W	430
L_b	95	W_a	250
L_c	55	W_b	160
L_d	55	W_c	65
L_e	15	S	15

reduces the complexity of the EM simulations. Based on the formula proposed in work [11], the equivalent dielectric constant of the two-layer substrate can be accurately estimated as given in (1).

$$\varepsilon_{req} = \left(\sum_{n=1}^{N} h_n\right) \cdot \left(\sum_{n=1}^{N} \frac{h_n}{\varepsilon_{rn}}\right)^{-1} \tag{1}$$

where h_n is the height of the nth substrate layer and ε_{rn} is the permittivity of the nth substrate layer. The thickness of the equivalent substrate is taken to equal the total height of the substrates and is given by (2).

$$h_{eq} = \left(\sum_{n=1}^{N} h_n\right) \tag{2}$$

After determining the equivalent dielectric constant ε_{req}, the filters are characterized by full-wave simulator softwares Ansoft$^{\text{TM}}$ High Frequency Structure Simulator (HFSS) and Agilent$^{\text{TM}}$ Advanced Design System (ADS) Momentum. Figures 1(c) and 2(c) depict the final layout of the FGCPW LPF and BPF. Tables 1 and 2 illustrate the dimensions of the LPF and BPF, respectively. The lengths of these two filters are 430 μm, which equals $0.3\lambda_g$ at 60 GHz. Such compact filters give low insertion loss on the lossy substrate.

2.2. ABCD Matrix Analysis and Equivalent Circuit Model

Figure 3(a) displays the lumped equivalent-circuit model of the proposed FGCPW filter which comprises eight unit-cells. The model can be divided into three parts: two series stubs (Z_2), two shunt stubs (Z_3), and four shunt stubs ($Y_{1\text{-}1}$). Since the circuit is symmetric with respect to the center, the equivalent circuit model can be simplified as shown in Figure 3(b), this model can be described conveniently as one

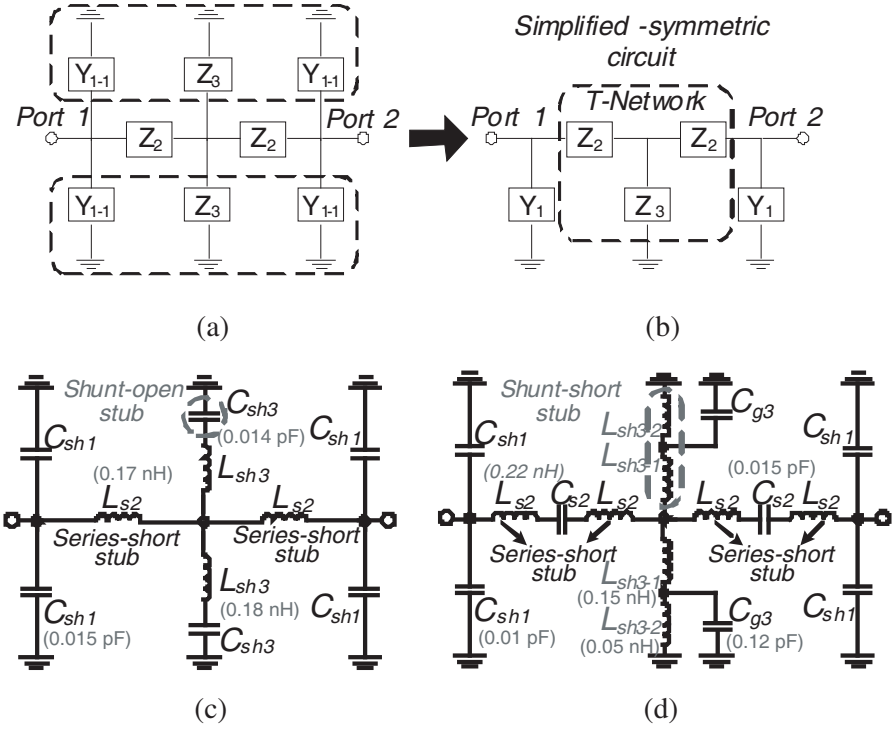

Figure 3. Lumped equivalent-circuit model of the (a) FGCPW filter, (b) simplified FGCPW filter, (c) LPF, and (d) BPF topologies.

T-network of impedance (Z parameters) at the center, and two shunt admittances (Y parameters) at the both ends. The corresponding ABCD matrix of the equivalent-circuit for both LPF and BPF is determined by (3).

$$\begin{aligned}\begin{bmatrix} A & B \\ C & D \end{bmatrix} &= \begin{bmatrix} 1 & 0 \\ \frac{1}{Z_1} & 1 \end{bmatrix} \begin{bmatrix} 1+\frac{Z_2}{Z_3} & 2Z_2+\frac{Z_2^2}{Z_3} \\ \frac{1}{Z_3} & 1+\frac{Z_2}{Z_3} \end{bmatrix} \begin{bmatrix} 1 & 0 \\ \frac{1}{Z_1} & 1 \end{bmatrix} \\ &= \begin{bmatrix} 1+\frac{Z_2(Z_1+Z_2+2Z_3)}{Z_1Z_3} & Z_2\left(2+\frac{Z_2}{Z_3}\right) \\ \frac{(Z_1+Z_2)^2+2Z_3(Z_1+Z_2)}{Z_1^2Z_3} & 1+\frac{Z_2(Z_1+Z_2+2Z_3)}{Z_1Z_3} \end{bmatrix} \end{aligned} \quad (3)$$

Figure 3(c) shows the equivalent circuit of the FGCPW LPF which correspondent values of Z_1, Z_2, and Z_3 are given by Eqs. (4a)–(4c).

$$Z_1 = \frac{1}{Y_1} = \frac{1}{j2\omega C_{sh1}} \tag{4a}$$

$$Z_2 = j\omega L_{s2} \tag{4b}$$

$$Z_3 = j\omega \frac{L_{sh3}}{2} + \frac{1}{j2\omega C_{sh3}} \tag{4c}$$

Figure 3(d) depicts the equivalent circuit of the FGCPW BPF. The values of Z_1, Z_2, and Z_3 are presented in (5a)–(5c).

$$Z_1 = \frac{1}{Y_1} = \frac{1}{j2\omega C_{sh1}} \tag{5a}$$

$$Z_2 = j2\omega L_{s2} + \frac{1}{j\omega C_{s2}} \tag{5b}$$

$$Z_3 = j\omega \frac{L_{sh3-1}}{2} + \left(j\omega \frac{L_{sh3-2}}{2} + \frac{1}{j2\omega C_{g3}} \right)^{-1} \tag{5c}$$

The ABCD matrix can be transferred to S-parameters to predict the frequency response. The transmission coefficient and its phase are shown in (6) and (7).

$$S_{21} = \frac{2}{A + B/Z_0 + CZ_0 + D} \tag{6}$$

$$\theta_{21} = \tan^{-1} \{ \mathrm{Im}\,(S_{21}) / \mathrm{Re}\,(S_{21}) \} \tag{7}$$

2.3. FGCPW LPF Design

As shown in Figure 3(c), the LPF is designed with two series inductors ($L_{s2} = 0.17\,\mathrm{nH}$), two shunted inductor-capacitor (LC) resonators ($L_{sh3} = 0.18\,\mathrm{nH}$ and $C_{sh3} = 0.014\,\mathrm{pF}$) at the center of the circuit, and two shunted capacitors ($C_{sh1} = 0.015\,\mathrm{pF}$) at both ends. The series inductor can be realized as a series-short-stub in FGCPW line. The shunted series LC resonator is realized as a narrow strip series with an open-stub in FGCPW line [12, 13]. The shunted capacitor can be easily realized as an open-stub in FGCPW line. The symmetrical layout keeps the circuit simply and compact.

2.4. FGCPW BPF Design

The BPF as shown in Figure 3(d) is designed with two series LC resonators ($L_{sh2} = 0.22\,\mathrm{nH}$ and $C_{sh2} = 0.015\,\mathrm{pF}$), two shunted LC resonators ($L_{sh3\text{-}1} = 0.15\,\mathrm{nH}$, $L_{sh3\text{-}2} = 0.05\,\mathrm{nH}$, and $C_g = 0.12\,\mathrm{pF}$) at

the center of the circuit, and two shunted capacitors ($C_{sh1} = 0.01\,\text{pF}$) at both ends. The series LC resonator is realized as two series-short-stubs and a capacitor in FGCPW line. The shunted inductor and capacitor are both realized as a short-stub and an open-stub in FGCPW line. The coupling gap between the signal line and ground plane is modeled as a capacitive element. C_g is the gap capacitance per unit length. The parasitic elements associated with these stubs and resonators need to be fine-tuned by EM simulator to fit the desired frequency response. The impedance of the input/output ports is designed to $50\,\Omega$ for minimizing the return loss, and being convenient for GSG probe contact during the measurement.

3. EXPERIMENTAL RESULTS

The chip photographs of the fabricated LPF and BPF are shown in Figures 4(a) and 4(b), respectively. The S-parameters were measured from 10 to 110 GHz. Figures 5(a) and 5(b) show the ideal equivalent-circuit frequency responses of the LPF and BPF, which provide the preliminary estimation for the circuit design. The thick substrate is suitable to implement CPW transmission line with low loss and wide impedance range [14]. On the other hand, the thick substrate may induce surface-wave-like (SWL) mode at low cut-off frequency. Therefore, the chosen substrate thickness should keep the circuits operating in CPW mode, meanwhile avoids exciting SWL propagation modes. Since the substrate thickness in WIN$^{\text{TM}}$ 0.15 µm pHEMT

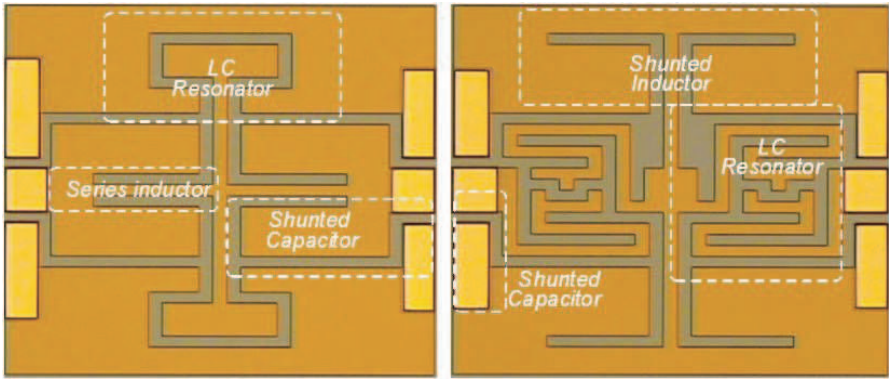

(a) (b)

Figure 4. The chip photographs of the fabricated FGCPW (a) LPF and (b) BPF, respectively.

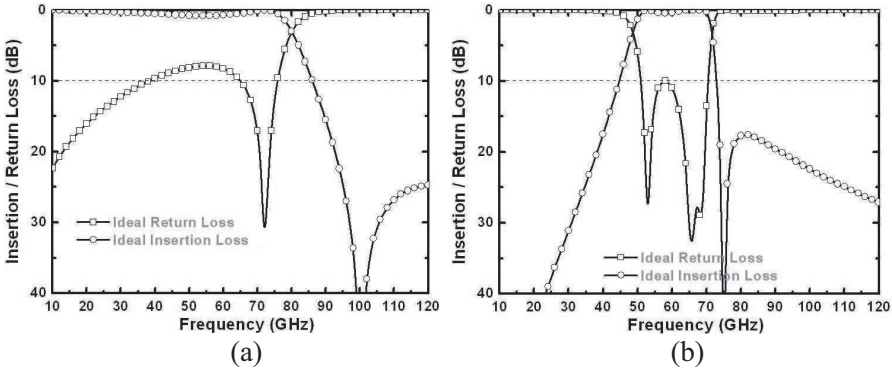

Figure 5. The ideal equivalent-circuit S-parameters of the FGCPW (a) LPF and (b) BPF.

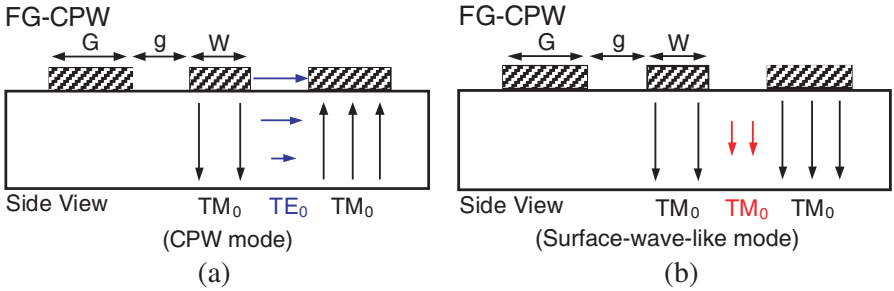

Figure 6. The electrical field distribution for the (a) CPW mode and (b) surface-wave-like mode, respectively.

process is fixed, the dimension of signal stripe width and gap of CPW line can be selected to guarantee CPW-mode operation. Work [15] suggested that the aspect ratio of $(W+2g)/H_{total}$ in CPW line should be kept less than 0.35 to avoid surface wave mode excitation, where W, g, and H_{total} are the signal stripe width, gap, and substrate thickness. Therefore, the maximal aspect ratio $(W+2g)/H_{total}$ of CPW line was accordingly chosen as 0.17 ($W = 55\,\mu$m, $g = 15\,\mu$m, and $H_{total} = 500.15\,\mu$m) to make the filters operate in CPW mode. A full-wave simulator software Ansoft^{TM} High Frequency Structure Simulator (HFSS) is performed to check this issue. Figures 6(a) and (b) plot the orientations of the electrical fields of the CPW and SWL modes. The field orientations in the outer region for the two modes are opposite [16]. As simulated field distribution shown in Figure 7(a), the dominant TE_0 CPW mode presents at 60 GHz. Figure 7(b) shows the

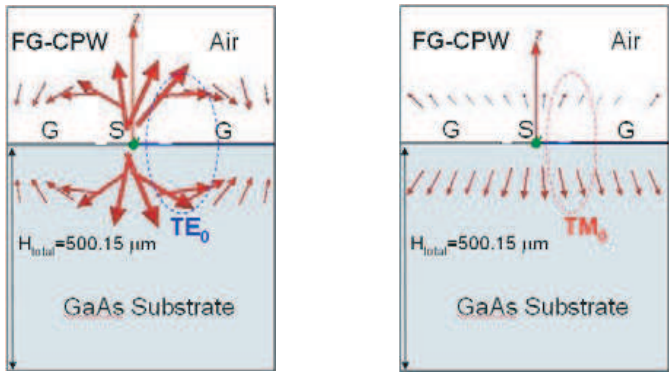

(a) (b)

Figure 7. The simulated electric field distribution of (a) CPW mode at 60 GHz and (b) surface-wave-like mode at 105 GHz in the proposed FGCPW filters, respectively. ($W = 55\,\mu m$, $g = 15\,\mu m$, and $H_{total} = 500.15\,\mu m$).

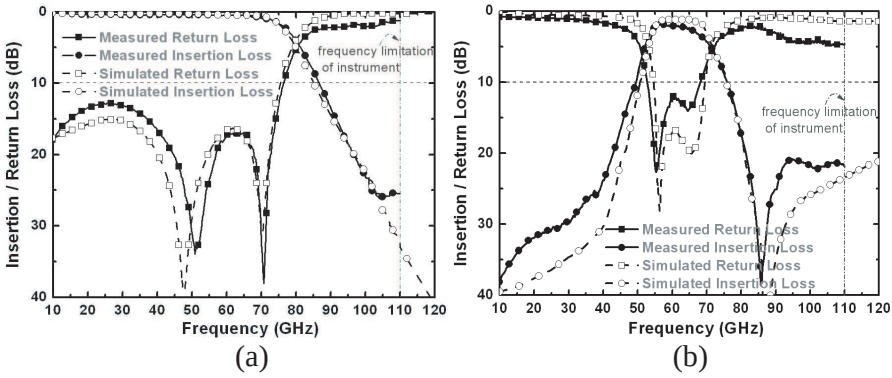

Figure 8. The simulated (full-EM simulations) and measured S-parameter of the FGCPW (a) LPF and (b) BPF.

electric field distribution of in the CPW line at 105 GHz, a coupling between the CPW mode and a SWL mode is observed. Figures 8(a) and 8(b) show the simulated (by full EM simulations) and measured frequency responses of the LPF and BPF. The measured and simulated S-parameters are in reasonably good agreements within the frequency band of interested, except that the SWL modes are excited at about 105 GHz for LPF and 95 GHz for BPF. The discrepancies are attributed to the excitations of the unwanted SWL propagation modes.

The measured minimum insertion loss in passband of the LPF and BPF are 0.5 dB and 1.5 dB, respectively. In the transition band,

very sharp frequency roll-off is observed at both the lower and upper passband edges. A sharp attenuation of 20 dB is achieved from 75 GHz to 95 GHz in the LPF and from 42 GHz to 55 GHz, and from 70 to 82 GHz in the BPF. As observed, a transmission zero located at 86 GHz achieves the attenuations greater than 38 dB, which is caused by the shunted LC resonator in the BPF. As for the stopbands, very wide rejections greater than 20 dB are observed at the out-of-band from 95 to 120 GHz in the LPF, and from 0 to 42 GHz, and from 82 to 120 GHz in the BPF. The return losses at 60 GHz of the LPF and BPF are greater than 12 dB and 13 dB, respectively. The measured 1-dB lower and upper cutoff frequencies of the LPF and BPF are from 0 to 70 GHz and from 55 to 66 GHz, respectively. The corresponding 1-dB bandwidths of the proposed LPF and BPF are greater than 200% and 18%, respectively.

As the spurious harmonics in RF transceiver can seriously degrade the system performance, the filter must reject the unwanted harmonics. The measured second harmonics at 120 GHz are approximately 25 and 20 dB in the LPF and BPF, respectively, indicating good harmonic suppression performance.

The simulated and measured group delays of the LPF and BPF are shown in Figures 9(a) and (b). The group delays in the passbands vary from 0 ns to 0.02 ns in LPF and from 0 ns to 0.05 ns in BPF, which make them possible to communicate without the signal distortion due to excellent phase linearity. Table 3 compares the performance of the proposed filters to recently published work on V-band on-chip designs [7–10]. As indicated, the proposed filters feature better low insertion, higher stopband and harmonics rejection, and smaller size than previous cited MMW filter designs.

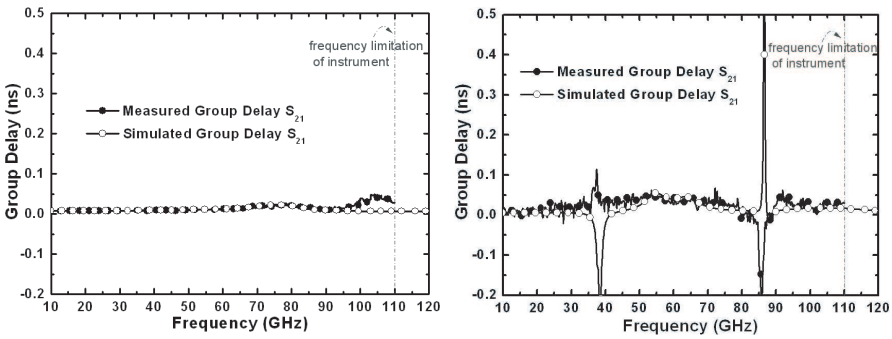

Figure 9. The simulated and measured group delays of the FGCPW (a) LPF and (b) BPF.

Table 3. Performance comparisons of the recently published V-band on-chip filters.

Reference		This Work 1	This Work 2	[7] MAP 2008	[7] MAP 2008	[8] EDL 2008	[9] AWPL 2005	[10]EuMC 2008
Process		GaAs 0.15 μm	GaAs 0.15 μm	CMOS 0.13 μm	CMOS 0.13 μm	CMOS 0.18 μm	LTCC	GaAs
Architecture / Sort		FGCPW / LPF	FGCPW / BPF	Microstrip / BPF	Microstrip / BPF	Microstrip / BPF	CPW-to-SL / BPF	Microstrip / BPF
Passband Frequency	(GHz)	0-70	55-66	59.5-68.5	57-66	58-70	59.5-62	45-75
Passband Bandwidth	(%)	200	18	14.1	14.6	18.8	3.7	50
Operation Frequency	(GHz)	60.5	60.5	64	61.5	64	60.75	60
Insertion Loss	(dB)	0.5	1.5	2.6	1.5	4.9	5	2.3
Return Loss	(dB)	12	13	8.5	9.5	10	16.5	16
Lower Attenuation Slope	(dB/10GHz)	0	23	26.7	41.9	21	30	22
Upper Attenuation Slope	(dB/10GHz)	10	24	10	10	22	16	22
2nd Harmonic Suppression	(dB)	25	22	11	10	20	NA	NA
Chip Size	(mm^2)	0.43×0.45	0.43×0.45	0.42×0.5	0.42×0.5	1.148 ×1.49	1.8×3.5	2×1

4. CONCLUSION

In this paper, two compact on-chip FGCPW LPF and BPF have been successfully developed with low insertion loss, high stopband and harmonic rejections. The compact size with 50 Ω FGCPW fed input/output ports make the filter easy integration with MMW transceiver for V-band multi-Gbps WPAN applications. The equivalent lumped-element circuit has been established based on an ABCD matrix. The representation of the ABCD matrix is obtained by consecutively multiplied ABCD matrixes of one T-network impedance and two shunt admittances. The LPF and BPF implemented in 0.15 μm pHEMT process obtain the insertion losses of better than 0.5 dB and 1.5 dB, and return losses of better than 12 dB and 13 dB, respectively. The 1-dB bandwidths are from 0 to 70 GHz in the LPF and from 55 to 66 GHz in the BPF. The stopband rejections are better than 20 dB from 95 to 120 GHz in the LPF, and from 0 to 42 GHz and 82 to 120 GHz in the BPF. The measured frequency responses show good agreements with the simulations. The chip size is very compact of $0.43 \times 0.45\,mm^2$. Hence, theses high performance filters can be widely used in integrated MMW transceivers.

ACKNOWLEDGMENT

This work was supported National Science Council (NSC) of the Republic of China under Contract No. NSC 96-2628-E-008-001-MY3. The authors would like to thank constant support from the Chip Implementation Center (CIC) of National Applied Research Laboratories.

REFERENCES

1. Smulders, P., "Exploring the 60 GHz band for local wireless multimedia access: Prospects and future directions," *IEEE Commun. Mag.*, Vol. 40, No. 1, 140–147, Jan. 2002.
2. Wu, M.-S., Y.-Z. Chueh, J.-C. Yeh, and S.-G. Mao, "Synthesis of triple-band and quad-band bandpass filters using lumped-element coplanar waveguide resonators," *Progress In Electromagnetics Research B*, Vol. 13, 433–451, 2009.
3. Chen, M., Y.-C. Lin, and M.-H. Ho, "Quasi-lumped design of bandpass filter using combined cpw and microstrip," *Progress In Electromagnetics Research Letters*, Vol. 9, 59–66, 2009.
4. Ismail, A., M. S. Razalli, M. A. Mahdi, R. S. A. R. Abdullah, N. K. Noordin, and M. F. A. Rasid, "X-band trisection substrate-integrated waveguide quasi-elliptic filter," *Progress In Electromagnetics Research*, PIER 88, 133–145, 2008.
5. Zhang, J. and T. Y. Hsiang, "Dispersion characteristics of coplanar waveguides at subterahertz frequencies," *Journal of Electromagnetic Waves and Application*, Vol. 20, No. 10, 1411–1417, 2006.
6. Wang, J.-P., B.-Z. Wang, and W. Shao, "A novel partly shielded finite ground CPW low pass filter," *Journal of Electromagnetic Waves and Application*, Vol. 19, No. 5, 689–696, 2005.
7. Yang, B., E. Skafidas, and R. J. Evans, "Design of 60 GHz millimetre-wave bandpass filter on bulk CMOS," *IET Trans. Microwaves, Antennas and Propagat.*, Vol. 3, No. 6, 943–949, Sep. 2009.
8. Hsu, C.-Y., C.-Y. Chen, and H.-R. Chuang, "A 60-GHz millimeter-wave bandpass filter using 0.18-μm CMOS technology," *IEEE Electron Device Lett.*, Vol. 29, No. 3, 246–248, Mar. 2008.
9. Lee, Y.-C., W.-I. Chang, and C.-S. Park, "Monolithic LTCC SiP transmitter for 60GHz wireless communication terminals," *IEEE MTT-S Int. Microwave Symp. Dig.*, 1015–1018, Jun. 2005.
10. Lee, M.-G., T.-S. Yun, K.-B. Kim, D.-H. Shin, T.-J. Baet, and

J.-C. Lee, "Design of millimeter-wave bandpass filters with $\lambda_g/4$ short stubs using GaAs surface micromachining," *European Int. Microwave Conf. Dig.*, Vol. 2, Oct. 4–6, 2005.

11. Ali, W. K. W. and S. H. AI-Charchafchi, "Using equivalent dielectric constant to simplify the analysis of patch microstrip antenna with multi layer substrates," *Proc. IEEE AP-S Int. Symp.*, Vol. 2, 676–679, Jun. 1998.
12. Hettak, K., N. Dib, A. F. Sheta, and S. Toutain, "A class of novel uniplanar series resonators and their implementation in original applications," *IEEE Trans. Microw. Theory Tech.*, Vol. 46, No. 9, 1270–1276, Sep. 1998.
13. Hettak, K., N. Dib, A. Omar, G. Y. Delisle, M. Stubbs, and S. Toutain, "A useful new class of miniature CPW shunt stubs and its impact on millimeter-wave integrated circuits," *IEEE Trans. Microw. Theory Tech.*, Vol. 47, No. 12, 2340–2349, Dec. 1999.
14. Simons, R. N., *Coplanar Waveguide Circuits Components and Systems*, Wiley-Interscience, 2001.
15. Godshalk, E. M., "Generation and observation of surface waves on dielectric slabs and coplanar structures," *IEEE MTT-S Int. Microwave Symp. Dig.*, 923–926, 1993.
16. Tsuji, M., H. Shigesawa, and A. A. Oliner, "New surface-wave-like mode on CPWs of infinite width and its role in explaining the leakage cancellation effect," *IEEE MTT-S Int. Microwave Symp. Dig.*, 495–498, 1992.